ARTICLE

Controlled Propulsion and Cargo Transport of Rotating Nickel Nanowires near a Patterned Solid Surface

Li Zhang,[†,*] Tristan Petit,[†,‡] Yang Lu,[§] Bradley E. Kratochvil,[†] Kathrin E. Peyer,[†] Ryan Pei,[§] Jun Lou,[§] and Bradley J. Nelson[†]

[†]Institute of Robotics and Intelligent Systems, ETH Zurich, CH-8092 Zurich, Switzerland, [‡]Université de Toulouse, ISAE, F-31055 Toulouse, France, and [§]Department of Mechanical Engineering and Materials Science, Rice University, Houston, Texas 77005, United States

ABSTRACT We show that rotating Ni nanowires are capable of propulsion and transport of colloidal cargo near a complex surface. When dissimilar boundary conditions exist at the two ends of a nanowire, such as when a nanowire is near a wall, tumbling motion can be generated that leads to propulsion of the nanowire. The motion of the nanowire can be precisely controlled using a uniform rotating magnetic field. We investigate the propulsion mechanism and the trajectory of the nanowire during the tumbling motion and demonstrate cargo transport of a polystyrene microbead by the nanowire over a flat surface or across an open microchannel. The results imply that functionalized, ferromagnetic one-dimensional, tumbling nanostructures can be used for cell manipulation and targeted drug delivery in a low Reynolds number aqueous environment.

KEYWORDS: Ni nanowire · propulsion · cargo transport · low Reynolds number · uniform rotating magnetic field

The propulsion of micro- and nanomachines in a low Reynolds number regime is challenging because inertia is negligible and viscous forces dominate locomotion at these small scales.[1−4] Purcell stated that a nonreciprocal motion is required for propulsion in low Reynolds numbers and postulated his "scallop theorem" in which a scallop-like hinged open/close mechanism would yield no net motion at very small scales because of the reciprocal nature of the mechanism.[1] Subsequently, various artificial microswimmers based on nonreciprocal motion have been realized. For example, one strategy is to mimic the swimming motion of natural microorganisms, such as spermatozoa[5] and *Escherichia coli*,[6,7] which are self-propelled by deforming a flexible flagellum or rotating a helically shaped flagellum.[8,9] Alternatively, artificial swimmers driven by chemical fuel from their environment have been realized by nanorods[10] and rolled-up microtubes,[11,12] which are capable of propulsion with a high velocity, *i.e.*, more than 50−100 body lengths per second and of transport of micro-objects by pushing or pulling.[13−17] Boundary conditions play an important role as the swimmers are near a solid surface. Lauga *et al.* reported that *E. coli* swim in circles as they approach a solid surface,[18] and we reported that swimming artificial bacterial flagella drift sidewise near a wall.[19] Contrary to the wall effect that impacts the propulsion of these swimmers, Tierno *et al.* reported a swimming mechanism resulting from a solid boundary in which a precessing magnetic field around an axis parallel to the boundary surface was applied to actuate a 3.8 μm long paramagnetic colloidal doublet swimmer with a maximum velocity of 3.2 μm/s.[20]

In this paper, we report swimming performance and colloidal cargo transport with nickel nanowires near a patterned solid surface driven by a uniform rotating magnetic field. The results show that the nanowires can be propelled and steered by a tumbling motion, *i.e.*, rotation plus translation. The propulsion mechanism and the trajectory of the nanowire during tumbling motion are also investigated. Moreover, as opposed to the transport of cargo by translational pushing or pulling,[13,14] the swimming velocity of a tumbling nanowire with assembled cargo is not significantly reduced, which indicates that the cargo assists the propulsion of this one-dimensional (1-D) slender body near a surface. Controlled swimming of nanowires and nanowire-microbead doublets upward or downward along the wall of microchannels is also possible, and they can swim near a surface with an arbitrary orientation. This tumbling motion provides a wireless manipulation method to propel 1-D magnetic nanostructures, such as nanowires and nanotubes, with or without cargo near a solid surface. If the 1-D ferromagnetic nanostructures are functionalized, then these swimmers have

*Address correspondence to lizhang@ethz.ch.

Received for review August 1, 2010 and accepted September 20, 2010.

Published online September 27, 2010. 10.1021/nn101861n

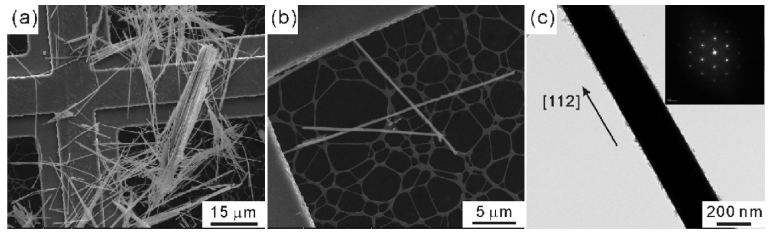

Figure 1. (a) SEM image of free-standing Ni nanowires on TEM grids. (b) SEM image of individual free-standing Ni nanowires with a diameter of *ca.* 200 nm. (c) TEM image of an as-fabricated Ni nanowire with a diameter of 260 nm. Inset: TEM electron diffraction pattern (EDP) of this Ni nanowire taken from (111) zone axis, showing that it is a single crystal and grows along the [112] direction.

potential for cell manipulation and targeted drug delivery in aqueous environments.[21−23]

RESULTS AND DISCUSSION

Ni nanowires were synthesized by a template-assisted electrochemical deposition method (see Materials and Methods Section). Scanning electron microscopy (SEM) micrographs show that the length of the as-fabricated nanowires is in the range of 10−30 μm (see Figure 1a and b). Transmission electron microscopy (TEM) investigation of individual nanowires indicates that the diameter of the nanowires is approximately 200 nm, and they are single crystalline with the growth direction of [112], as shown in Figure 1c. For precise control of the motion of the nanowires under an optical microscope, a uniform rotating magnetic field was generated by three orthogonal electromagnetic coil pairs, which have also been used for precise control of the swimming of artificial bacterial flagella in 3-D.[7,19,24]

A rotating magnetic field applied in a horizontal plane is shown in Figure 2a in which the nanowires simply rotate in this plane due to the induced magnetic torque (τ_m), which is consistent with previous reports.[25,26] Experimental results also show that at these low Reynolds numbers, *i.e.*, $10^{-4}-10^{-5}$, the nanowires start or stop moving instantly as the magnetic field is turned on or off. Thus, the nanowires precisely follow the magnetic field with their long axis in the horizontal plane. To generate propulsion, a simple rotational motion of a nanowire is not sufficient, and asymmetric boundary conditions are applied to break the time reversibility of the motion.[20] To observe the propulsion of a rotating nanowire in the horizontal $X-Y$ plane, the nanowire was placed near a vertical wall inside a microchannel, as shown in Figure 2b. It is found that, though a gap exists between the rotating nanowire and the vertical wall, the nanowire is propelled with a tumbling motion indicating that the propulsion results from the vertical boundary. Moreover, the propulsion direction of the nanowire is reversed by reversing the rotational direction of the applied magnetic field (see video S1 in Supporting Information). It is known that the drag coefficient of an object increases when it approaches a wall.[8,27] Therefore, in the case as depicted in Figure 2c, if a nanowire rotates with an angular speed of ω, then the hydrodynamic interaction of the nanowire with the wall is stronger on the "b" end than that on the "a" end, leading to a velocity difference between the two ends of the nanowire, *i.e.*, $v_a > v_b$. The center of rotation of the nanowire changes during tumbling due to the dynamic boundary condition. When the long axis of the nanowire is parallel to the wall, the center of rotation overlaps with the center of mass of the nanowire due to the symmetric boundary condition along the nanowire; while with other orientations of the nanowire the center of rotation moves to the side of the center of mass which is closer to the wall due to the asymmetric boundary condition. This simplified model shows why a rotating nanowire can be propelled near a wall. Swimming tests in 2-D were performed near a flat Si surface, shown schematically in Figure 3a. The parameter "α" in Figure 3a indicates the orientation of the vector **A** in the $X-Y$ plane, which is perpendicular to the vertical plane of rotation of the magnetic field. (In the videos S2 and S3 in Supporting Information, the vector **A** is represented by the "compass needle" symbol.) In order to steer the tumbling motion near a solid boundary only the input param-

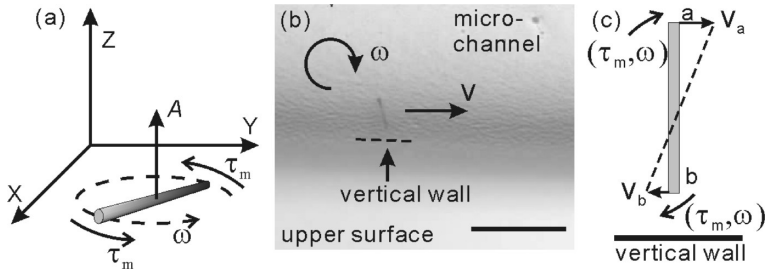

Figure 2. (a) Schematic of a nanowire rotating horizontally in the $X-Y$ plane. (b) A nanowire is propelled near a vertical wall (also see video S1 in Supporting Information). The scale bar is 50 μm. (c) Schematic showing that, due to inhomogeneous boundary conditions, the velocities at the two ends of the nanowire are different, *i.e.*, $v_a > v_b$.

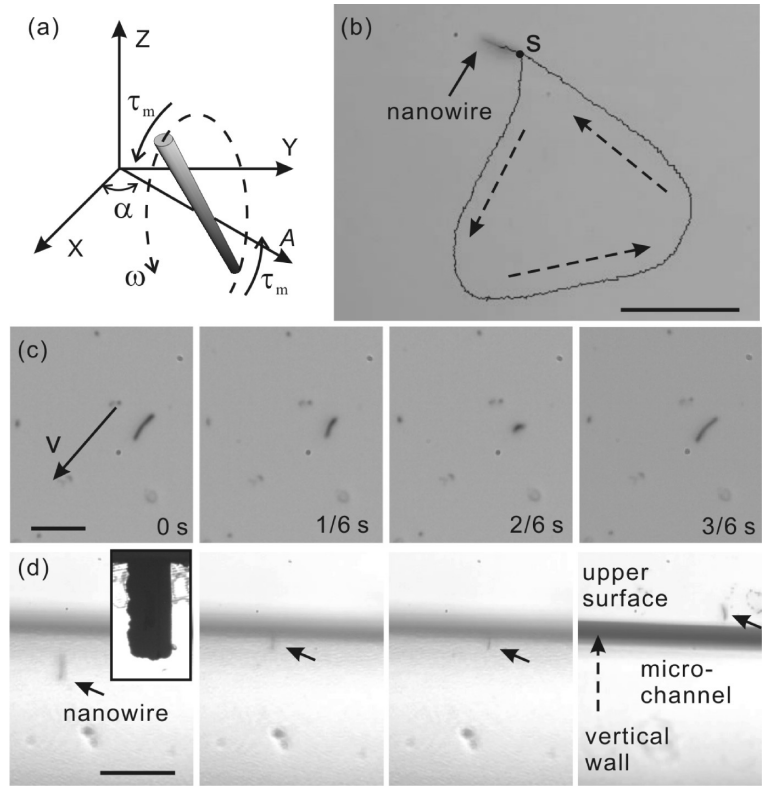

Figure 3. (a) Schematic of a nanowire rotating vertically with respect to the *X*−*Y* plane. (b) The nanowire travels along the tracking line near a flat surface, (also see video S2 in Supporting Information). The scale bar is 50 μm. (c) A series of frames showing that a nanowire is propelled near a horizontal wall. The scale bar is 20 μm. (d) Time-lapse images showing the upward propulsion of a 12 μm long nanowire along a vertical wall inside a microchannel and, eventually, on the upper surface outside the channel (also see video S3 in Supporting Information). The input frequency is 6 Hz. Inset: Optical microscope image shows the cross-section of the 55 μm deep microchannel. The scale bar is 50 μm.

eter α has to be changed. The plane of rotation of the magnetic field is updated, and the plane of rotation of the nanowire instantaneously follows due to the lack of inertial effects. Therefore, the propulsion direction is controlled. Figure 3b shows the tracking line of a 17 μm long nanowire swimming near a flat surface. At the end it crosses the initial starting point "S", which indicates that steering is precisely controlled in 2-D. Figure 3c presents the time-lapse images of an actuated nanowire near a horizontal surface with different orientations from a top view. Unlike artificial helical microswimmers near a solid surface,[19,24] sidewise drifting of a straight nanowire with tumbling motion is negligible because the propulsion direction is in the same plane as the rotating plane.

Climbing tests are also conducted near a vertical wall in which a 12 μm long nanowire was propelled toward a 55 μm high vertical wall in a microchannel, as shown in Figure 3d. The results show that the nanowire can overcome its weight and tumble upward along the vertical wall of the channel. After the nanowire swims out of the channel, the propulsion direction is reversed by inversing the rotational plane of the magnetic field, and the nanowire moves back into the channel (see video S3 in Supporting Information). Moreover, the swimming time to cross a vertical wall by upward and downward motion is approximately 14 ± 1 and 15 ± 1 s, respectively, which implies that the influence of the gravitational force of the nanowire on its propulsion is negligible. For example, the total weight of the 12 μm long Ni nanowire with a diameter of 200 nm is approximately 3.2×10^{-2} pN (the density of Ni is 8.9 g/cm^3). The difference in the swimming time is mainly attributed to the varying roughness of the vertical wall surface prepared by deep reactive-ion etching (DRIE) process. Unlike swimmers capable of swimming in 3-D, the tumbling nanowires pass an obstacle "automatically" by moving along the surface, which demonstrates the feasibility of propelling these 1-D nanostructures near a complex-patterned surface.

To measure the average translational velocity of the nanowires under a particular magnetic field strength and frequency, we maintained the steering parameter (α) at a constant value and measured the translational displacement of the individual nanowire in the horizontal *X*−*Y* plane. The dependence of the average translational velocity (v) of nanowires with different lengths on the rotation frequency was characterized. The input frequency was increased from 1 Hz to a maximum 50 Hz, as shown in Figure 4. The result shows the linear relation between the input frequency and v when the nanowire rotates in sync with the input field.

For a 10 μm long nanowire in a 0.5 mT field, the measured maximum *v* is approximately 26 μm/s at 35 Hz; increasing the frequency further reduces the velocity gradually because the available magnetic torque is no longer sufficient to keep the rotation of the nanowire synchronized with the applied field. This maximum synchronized frequency is referred to as the step-out frequency which also exists for artificial helical swimmers actuated by a rotating magnetic field.[7,28] With the same applied magnetic field strength (*i.e.*, 0.5 mT), the step-out frequency of a 4 μm long nanowire is higher which is attributed to the fact that a shorter nanowire encounters less fluidic drag forces compared to that of a longer one. To increase the step-out frequency for a higher maximum propulsion velocity, a higher field strength can be applied as shown in Figure 4 for the same 10 μm long nanowire but with a 5 mT field strength. In our experiments, the highest *v* for the 4 and 12 μm long nanowires is 17 (*ca.* 4 body lengths/s) and 37 μm/s (*ca.* 3 body lengths/s), respectively, though the step-out frequency was not reached in the tested frequency range. Figure 4 also shows that when the input frequency is larger than 20 Hz there are fluctuations in *v* which are not due to step-out but primarily to nonhomogeneous surface roughness.

For Stokes flow, the tumbling motion of a nanowire can be considered to be a succession of equilibrium positions. There are two torques acting on the nanowire that counterbalance each other: the magnetic driving torque and the torque induced by the drag force. We assume that the nanowire is rotating in sync with the rotating magnetic field and that its structure is not deformable so that the rotational velocity of the nanowire is the same as the input rotational velocity of the magnetic field. The drag force at both extremities of the nanowire can then be calculated. To generate propulsion, the velocities at the two extremities should be different, as shown in Figure 2c. The velocity is related to the drag force depending on the geometry of the nanowire and its relative position and orientation to the wall. Assuming that the nanowire behaves like a slender body near a wall, the singularity method is appropriate for estimating instantaneous velocity distributions.[29,30] Thus, the forces applied on the nanowire can be modeled as a linear distribution of singularities, and the instantaneous velocities due to the fluidic interaction with the wall during a complete rotation of the nanowire can be obtained (see Supporting Information). Calculations were conducted with a rotating frequency of 1 Hz for a 12 μm long nanowire with a diameter of 200 nm and with an initially horizontal orientation. The distance of the horizontal nanowire to the wall is set to 6.5 μm to correspond to experimental velocities, which is also comparable with the condition of a paramagnetic doublet swimmer floating above a glass surface.[20] It was found that the trajectory of the center of mass, *i.e.*, the center of the nanowire, is a prolate cycloid, as shown in Figure 5a. Its parametric equations are given by:

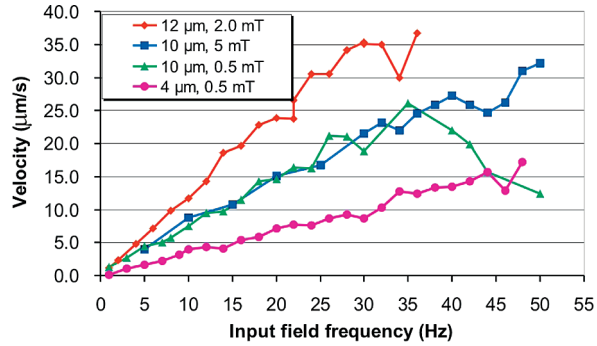

Figure 4. Average translational velocity plot for different lengths of nanowires and magnetic field strengths with respect to the input field frequency.

$$x = \frac{l_{eq}}{2\pi}(2\phi - (1 + \delta)\sin(2\phi)) \quad (1)$$

$$z = h_{hor} + \frac{l_{eq}}{4}(1 - \cos(2\phi)) \quad (2)$$

where h_{hor} is the height when the nanowire is horizontal, φ the inclination of the nanowire equals $\varphi = \omega t + \varphi_0$ with ω being the angular frequency, *t* being the time, and φ_0 being the initial phase, l_{eq} is the equivalent length of the nanowire, and δ is a dimensionless parameter.[31] For a tumbling motion with the highest propulsion efficiency, *i.e.*, a nanowire tumbling on a solid surface without slipping, the nanowire advances for two body lengths in one revolution, and the corresponding trajectory is a perfect cycloid without backward motion, and its parametric equation is given by eqs 1 and 2 with $h_{hor} = \delta = 0$ and l_{eq} equal to the length of the nanowire. However, modeling results show that the nanowire tumbling above the surface is far from this maximum-propulsion efficiency case, as its equivalent length is equal to l_{eq} = 560 nm, h_{hor}= 6.5 μm, and δ = 0.03. The trajectory of its center of mass is equivalent to a 560 nm long nanowire tumbling with approximately

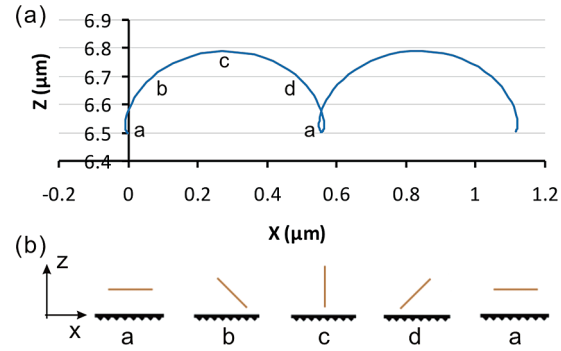

Figure 5. (a) Trajectory of the center of mass of a rotating single nanowire near a wall. We assume that the horizontal 12 μm long nanowire has an initial distance of 6.5 μm from the wall and rotates with a frequency of 1 Hz. (b) Schematic diagram showing the orientation of the nanowire with tumbling motion with respect to the trajectory line of (a).

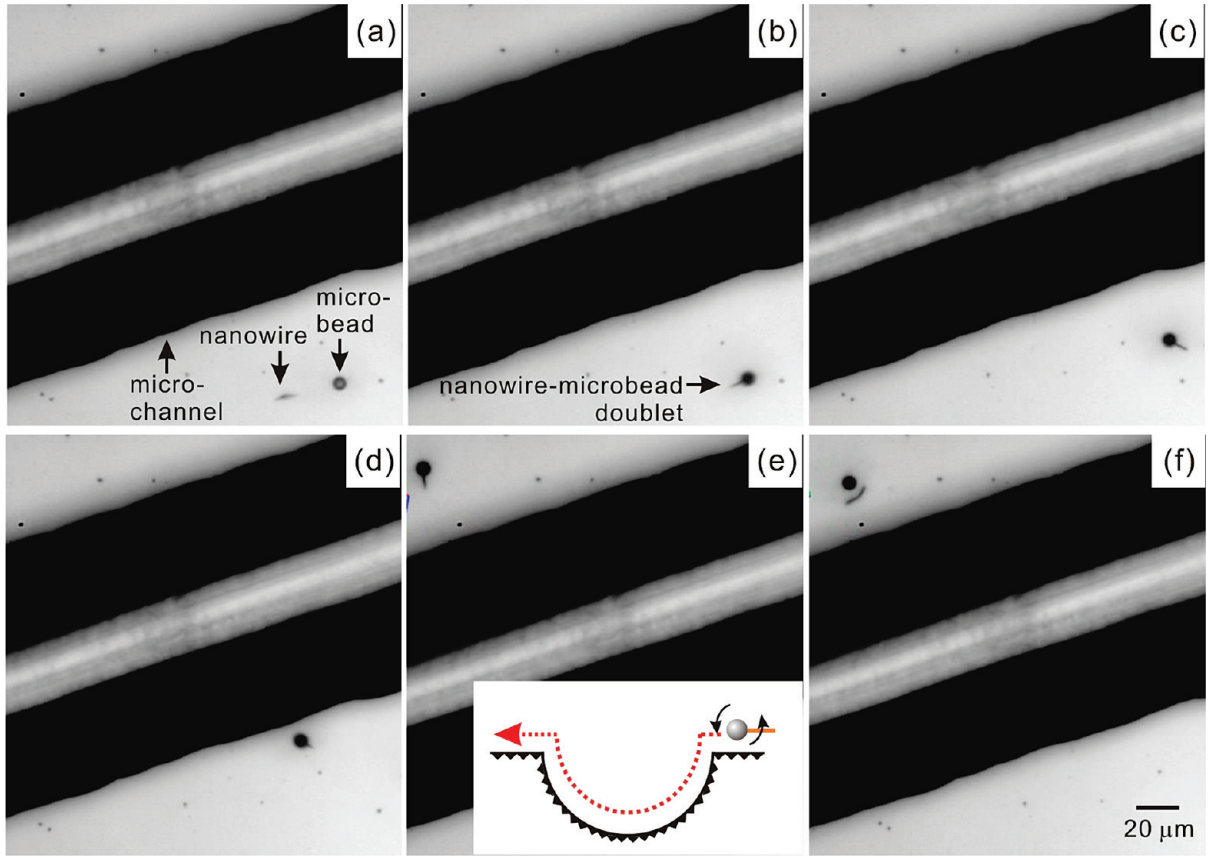

Figure 6. Pick-and-place of a 6 μm diameter PS micobead using an 11 μm long nanowire by tumbling (also see video S4). (a) A nanowire swims toward a 6 μm diameter microbead by tumbling motion. (b) The nanowire is assembled with the PS microbead, *i.e.*, nanowire-microbead doublet. (c) The doublet is steered to swim toward the microchannel. (d) The doublet is self-propelled near the microchannel. (e) The doublet crosses the channel and reaches the other upper-surface side of the channel. Inset: schematic of the side view of the doublet swimming across the channel. The width and the depth of the microchannel are 120 and 55 μm, respectively. (f) Disassembling of the doublet to the nanowire and the PS microbead by inversing the rotating direction and tuning the input frequency.

two body lengths per rotation on a plane 6.5 μm above the surface. When the nanowire is nearly parallel to the surface, the wall effect has an adverse effect, and the overall drag force generates a backward motion, reducing the average propulsion velocity.

For colloidal cargo transport using individual Ni nanowires, a 6 μm diameter polystyrene (PS) microbead was directly assembled onto one end of the nanowire by tumbling, then transported from one side of an open microchannel to the other side and released from the nanowire, as shown in Figure 6. First, the 11 μm long nanowire is propelled toward the microbead and assembled on it directly with a 31 Hz rotating frequency. The assembly is mainly attributed to penetration of the nanowire into the microbead, as the velocity at the end of the nanowire is sufficiently high (see Figure 6a and b). Then, the nanowire-microbead doublet is steered toward the microchannel, as shown in Figure 6c and d. The results show that the motion of the doublet can be controlled in a similar way to the single nanowire. After approximate 17 s, the doublet crosses the microchannel and reaches the other upper surface. Eventually, by reversing the rotating direction of the nanowire from counterclockwise to clockwise and tuning the rotational frequency, the doublet is disassembled into a nanowire and a microbead. A video clip is also available in the Supporting Information to show the pick-and-place process of the colloidal cargo using a nanowire (see video S4). The average propulsion velocity of these doublet structures was investigated for three different lengths of nanowires, 9, 11, and 13.6 μm. The dependence of the propulsive velocity of these doublets at different input frequencies is summarized in Table 1. Unlike pulling or pushing of a microbead using a catalytic nanowire motor,[13,14] in which the translational velocity of the doublet is significantly reduced due to the additional drag resistance from the cargo, our results show that the average translational velocity of the rotating nanowires with and without cargo is comparable. For the tumbling motion, cargo is rotated with the nanowire, hence, it significantly increases the drag difference at the two extremities of the nanowire. The large change of the drag at the extremity of the nanowire with the microbead is also revealed by rotating the doublet in the horizontal plane (see video S4, Supporting Information) in which the rotating radius of the microbead and the nanowire are *ca.* 2 and 4 μm, respectively. Apparently, the center

TABLE 1. Dependence of the Translational Velocity of Nanowire-Microbead Doublets on the Input Frequency

sample no.	length of nanowire before assembly	length of freestanding nanowire part (μm)	input frequency (Hz)	average translational velocity (v) of doublet (μm/s)
I	9	5.4	3.0	3.1
			4.0	4.1
II	11 (v = 40.8 μm/s at 31 Hz)	8.4	23.0	22.7
			31.0	31.5
III	13.6 ("v" shape, bent 135° at center of the nanowire)	12.0	3.0	5.0

of rotation of the doublet is nearer to the microbeads as the length of the nanowire becomes shorter.

In summary, a rotating magnetic field has been applied to propel Ni nanowires in water with a tumbling motion near a solid boundary. The maximum average translational velocity of 4−12 μm long nanowires is approximately 3−4 body lengths per second when the rotating frequency is less than 50 Hz. The rotating nanowires can be propelled and precisely steered near horizontal, vertical, or curved walls. Cargo transport by individual nanowires loaded with a 6 μm diameter microbead is investigated. The results show that the cargo assists the propulsion instead of simply adding resistance, therefore, it is an efficient approach for targeted cargo delivery near a patterned surface with arbitrary orientations. Once functionalized, the nanowires also have potential for drug delivery and intracellular sensing.

MATERIALS AND METHODS

Fabrication of Ni Nanowires. Ni nanowires were synthesized by a template-assisted electrochemical deposition method. Anodic aluminum oxide (AAO) membranes were used as the template in which there are ordered channels with pore sizes ranging from tens to hundreds of nanometers. One side of the AAO template was sputter coated with silver film and was then mounted on a copper plate as a working electrode. The counter electrode for electroplating is a graphite sheet. Ni nanowires were fabricated in a plating solution of $Ni(H_2NSO_3)_2$ purchased from Technic Inc. The length and the diameter of the nanowires are controlled by the electroplating time and the pore size of the AAO template, respectively. Eventually, freestanding Ni nanowires are obtained by wet etching of the AAO template in NaOH solution. The fabrication flow is shown in the Supporting Information. Ni nanowires with diameters of 30−300 nm can be obtained by this method, however for the magnetic manipulation experiments, nanowires with a diameter of *ca.* 200 nm are adopted for the sake of easy inspection and video capture under an optical microscope.

Magnetic Actuation of Ni Nanowires. In the experiments, three parameters were independently controlled in software by the user: the magnetic field strength (B), the rotational frequency (ω) of the field, and the steering parameter (α). A maximum field strength of 6.0 mT was generated. Before the magnetic actuation, the as-fabricated Ni nanowires were separated in DI water by a 15 min sonication. Afterward, the nanowire suspension was transferred into a tank 20 (length) × 15 (width) × 2 mm (height). A Si substrate with open microchannels, patterned by DRIE, was placed at the bottom of the tank for the swimming tests. The magnetic field was turned on after the nanowires sank near the Si substrate. In the experiments, the nanowires were actuated by a rotating field that was either parallel or perpendicular to the substrate. Details of the magnetic actuation of individual Ni nanowires is given in the Supporting Information.

Acknowledgment. We thank the FIRST lab of ETH Zurich for technical support. Funding for this research was partially conducted from the project "Nano-Actuators and Nano-Sensors for Medical Applications (NANOMA)" funded by the European Commission under the seventh Framework Program (FP7) and partially conducted by United States National Science Foundation ECCS 0702766.

Supporting Information Available: Schematic of the Ni nanowires fabrication, principle of magnetic actuation of Ni nanowires in water, and numerical modeling of the tumbling motion of a nanowire as well as four video clips can be found online. Video S1 shows that a rotating Ni nanowire is propelled with asymmetric boundary conditions. Video S2 shows the steering of a Ni nanowire near a horizontal surface with a tracking line. Video S3 shows a 12 μm long Ni nanowire climbing up and down along a 55 μm deep vertical wall, and video S4 shows pick-and-place of a PS microbead using a Ni nanowire. The 6 μm diameter microbead is transported from one side of an open microchannel to the other side. The red line indicates the commanded direction of the vector **A**. Yaw shows the value of the steering parameter α. The blue and green lines indicate the plane of rotation of the uniform magnetic field, in which the green line represents the direction of the input field. All swimming tests were conducted in DI water. This material is available free of charge *via* the Internet at http://pubs.acs.org.

REFERENCES AND NOTES

1. Purcell, E. M. Life at Low Reynolds-Number. *Am. J. Phys.* **1977**, *45*, 3–11.
2. Ozin, G. A.; Manners, I.; Fournier-Bidoz, S.; Arsenault, A. Dream Nanomachines. *Adv. Mater.* **2005**, *17*, 3011–3018.
3. Mallouk, T. E.; Sen, A. Powering Nanorobots. *Sci. Am.* **2009**, *300*, 72–77.
4. Abbott, J. J.; Peyer, K. E.; Lagomarsino, M. C.; Zhang, L.; Dong, L. X.; Kaliakatsos, I. K.; Nelson, B. J. How Should Microrobots Swim. *Int. J. Robot. Res.* **2009**, *28*, 1434–1447.
5. Dreyfus, R.; Baudry, J.; Roper, M. L.; Fermigier, M.; Stone, H. A.; Bibette, J. Microscopic Artificial Swimmers. *Nature* **2005**, *437*, 862–865.
6. Ghosh, A.; Fischer, P. Controlled Propulsion of Artificial Magnetic Nanostructured Propellers. *Nano Lett.* **2009**, *9*, 2243–2245.
7. Zhang, L.; Abbott, J. J.; Dong, L. X.; Kratochvil, B. E.; Bell, D. J.; Nelson, B. J. Artificial Bacterial Flagella: Fabrication and Magnetic Control. *Appl. Phys. Lett.* **2009**, *94*, 064107.
8. Lauga, E.; Powers, T. R. The Hydrodynamics of Swimming Microorganisms. *Rep. Prog. Phys.* **2009**, *72*, 096601.
9. Berg, H. C.; Anderson, R. A. Bacteria Swim by Rotating their Flagellar Filaments. *Nature* **1973**, *245*, 380–382.
10. Laocharoensuk, R.; Burdick, J.; Wang, J. Carbon-Nanotube-Induced Acceleration of Catalytic Nanomotors. *ACS Nano* **2008**, *2*, 1069–1075.
11. Solovev, A. A.; Mei, Y. F.; Urena, E. B.; Huang, G. S.; Schmidt, O. G. Catalytic Microtubular Jet Engines Self-Propelled by Accumulated Gas Bubbles. *Small* **2009**, *5*, 1688–1692.
12. Mei, Y. F.; Huang, G. S.; Solovev, A. A.; Urena, E. B.; Moench, I.; Ding, F.; Reindl, T.; Fu, R. K. Y.; Chu, P. K.; Schmidt, O. G.

Versatile Approach for Integrative and Functionalized Tubes by Strain Engineering of Nanomembranes on Polymers. *Adv. Mater.* **2008**, *20*, 4085–4090.
13. Burdick, J.; Laocharoensuk, R.; Wheat, P. M.; Posner, J. D.; Wang, J. Synthetic Nanomotors in Microchannel Networks: Directional Microchip Motion and Controlled Manipulation of Cargo. *J. Am. Chem. Soc.* **2008**, *130*, 8164–8165.
14. Sundararajan, S.; Lammert, P. E.; Zudans, A. W.; Crespi, V. H.; Sen, A. Catalytic Motors for Transport of Colloidal Cargo. *Nano Lett.* **2008**, *8*, 1271–1276.
15. Manesh, K. M.; Cardona, M.; Yuan, R.; Clark, M.; Kagan, D.; Balasubramanian, S.; Wang, J. Template-Assisted Fabrication of Salt-Independent Catalytic Tubular Microengines. *ACS Nano* **2010**, *4*, 1799–1804.
16. Sundararajan, S.; Sengupta, S.; Ibele, M. E.; Sen, A. Drop-Off of Colloidal Cargo Transported by Catalytic Pt-Au Nanomotors via Photochemical Stimuli. *Small* **2010**, *6*, 1479–1482.
17. Solovev, A. A.; Sanchez, S.; Pumera, M.; Mei, Y. F.; Schmidt, O. G. Nanomotors: Magnetic Control of Tubular Catalytic Microbots for the Transport, Assembly, and Delivery of Micro-Objects. *Adv. Funct. Mater.* **2010**, *20*, 2430–2435.
18. Lauga, E.; DiLuzio, W. R.; Whitesides, G. M.; Stone, H. A. Swimming in Circles: Motion of Bacteria near Solid Boundaries. *Biophys. J.* **2006**, *90*, 400–412.
19. Zhang, L.; Peyer, K. E.; Nelson, B. J. Artificial Bacterial Flagella for Micromanipulation. *Lab Chip* **2010**, *10*, 2203–2215.
20. Tierno, P.; Golestanian, R.; Pagonabarraga, I.; Sagues, F. Controlled Swimming in Confined Fluids of Magnetically Actuated Colloidal Rotors. *Phys. Rev. Lett.* **2008**, *101*, 218304.
21. Cai, D.; Mataraza, J. M.; Qin, Z. H.; Huang, Z. P.; Huang, J. Y.; Chiles, T. C.; Carnahan, D.; Kempa, K.; Ren, Z. F. Highly Efficient Molecular Delivery into Mammalian Cells Using Carbon Nanotube Spearing. *Nat. Methods* **2005**, *2*, 449–454.
22. Fan, D.; Yin, Z.; Cheong, R.; Zhu, F. Q.; Cammarata, R. C.; Chien, C. L.; Levchenko, A. Subcellular-Resolution Delivery of a Cytokine through Precisely Manipulated Nanowires. *Nat. Nanotechnol.* **2010**, *5*, 545–551.
23. Nelson, B. J.; Kaliakatsos, I. K.; Abbott, J. J. Microrobots for Minimally Invasive Medicine. *Annu. Rev. Biomed. Eng.* **2010**, *12*, 55–85.
24. Zhang, L.; Abbott, J. J.; Dong, L. X.; Peyer, K. E.; Kratochvil, B. E.; Zhang, H. X.; Bergeles, C.; Nelson, B. J. Characterizing the Swimming Properties of Artificial Bacterial Flagella. *Nano Lett.* **2009**, *9*, 3663–3667.
25. Keshoju, K.; Xing, H.; Sun, L. Magnetic Field Driven Nanowire Rotation in Suspension. *Appl. Phys. Lett.* **2007**, *91*, 123114.
26. Tanase, M.; Bauer, L. A.; Hultgren, A.; Silevitch, D. M.; Sun, L.; Reich, D. H.; Searson, P. C.; Meyer, G. J. Magnetic Alignment of Fluorescent Nanowires. *Nano Lett.* **2001**, *1*, 155–158.
27. De Mestre, N. J.; Russel, W. B. Low-Reynolds-Number Translation of a Slender Cylinder near a Plane Wall. *J. Eng. Math.* **1975**, *9*, 81–91.
28. Honda, T.; Arai, K. I.; Ishiyama, K. Micro Swimming Mechanisms Propelled by External Magnetic Fields. *IEEE Trans. Magn.* **1996**, *32*, 5085–5087.
29. Blake, J. R.; Chwang, A. T. Fundamental Singularities of Viscous-Flow 0.1. Image Systems in Vicinity of a Stationary No-Slip Boundary. *J. Eng. Math.* **1974**, *8*, 23–29.
30. Barta, E.; Liron, N. Slender Body Interactions for Low Reynolds-Numbers 0.1. Body-Wall Interactions. *SIAM J. Appl. Math.* **1988**, *48*, 992–1008.
31. When $\delta = 0$ there is no backward motion, and when $\delta > 0$ there is backward motion.